# Spectral Tuning of Ultraviolet Cone Pigments: An Interhelical Lock Mechanism

Sivakumar Sekharan[†*], Victoria L. Mooney[†], Ivan Rivalta[†], Manija A. Kazmi[‡], Maureen Neitz[§], Jay Neitz[§], Thomas P. Sakmar[‡], Elsa C. Y. Yan[†*], Victor S. Batista[†,*]

[†]Department of Chemistry, Yale University, P.O. Box 208107, New Haven, CT 06520-8107
[†]Laboratory of Chemical Biology and Signal Transduction, Rockefeller University, New York, NY 10065
[§]School of Medicine, Department of Ophthalmology, University of Washington, Seattle, WA 98195

**ABSTRACT**: Ultraviolet (UV) cone pigments can provide insights into the molecular evolution of vertebrate vision since they are nearer to ancestral pigments than the dim-light rod photoreceptor rhodopsin. While visible-absorbing pigments contain an 11-*cis* retinyl chromophore with a protonated Schiff-base (PSB11), UV pigments uniquely contain an unprotonated Schiff-base (USB11). Upon F86Y mutation in model UV pigments, both the USB11 and PSB11 forms of the chromophore are found to co-exist at physiological pH. The origin of this intriguing equilibrium remains to be understood at the molecular level. Here, we address this phenomenon and the role of the USB11 environment in spectral tuning by combining mutagenesis studies with spectroscopic (UV/Vis) and theoretical [DFT-QM/MM (SORCI+Q//B3LYP/6-31G(d): Amber96)] analysis. We compare structural models of the wildtype (WT), F86Y, S90A and S90C mutants of *Siberian Hamster* ultraviolet (SHUV) cone pigment to explore structural rearrangements that stabilize USB11 over PSB11. We find that the PSB11 forms upon F86Y mutation and is stabilized by an *"inter-helical lock"* (IHL) established by hydrogen bonding networks between transmembrane (TM) helices TM6, TM2 and TM3 (including water w2c and amino acid residues Y265, F86Y, G117, S118, A114 and E113). The findings implicate the involvement of the IHL in constraining the displacement of TM6, an essential component of the activation of rhodopsin, in the spectral tuning of UV pigments.

During the molecular evolution of vertebrate vision, the ultraviolet (UV) cone pigment acquired structural and functional features that are transitional between those of long-wavelength cone and rhodopsin rod photoreceptors. Five classes of visual pigments have evolved (Fig. 1A), including rhodopsin (RH1, 460–530 nm), rhodopsin-like (RH2, 450–535 nm), short wavelength-sensitive 1 and 2 (SWS1, 355–440 nm; SWS2, 400–490 nm), and medium/long wavelength-sensitive (M/LWS, 490–570 nm).[1-6] In mammals, UV and violet SWS1 cone pigments are the immediate predecessors of rhodopsin (Fig. 1A), since modern-day mammals no longer have functional SWS2 pigments. Rhodopsin absorbs in the visible region and contains a protonated Schiff base of 11-*cis*-retinal (PSB11), whereas UV pigments contain an unprotonated Schiff base (USB11) linked to a conserved lysine residue. The structural factors that determine this distinct protonation state of the chromophore in UV pigments, remains to be understood at the molecular level. Here, we address these fundamental structure/function relations in the Siberian hamster (*Phodopus sungorus*) UV (SHUV) cone photoreceptor.

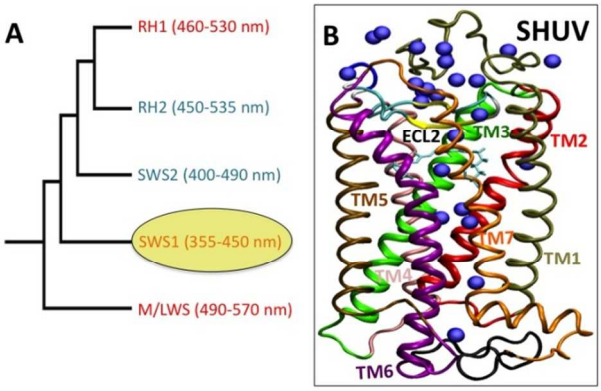


**Figure 1.** Panel A: Cladogram depicting the evolution of the five classes of vertebrate visual pigments. Classes shown in blue are no longer expressed in non-monotreme mammals. The SHUV pigment is classified under the SWS1 category highlighted in yellow. Panel B: DFT-QM/MM structural model of the wild-type SHUV pigment, with water molecules (blue spheres) and seven transmembrane helices TM1-TM7 (labeled cartoon) built as a homology model using the X-ray structure of bovine rhodopsin (PDB code: 1U19) as template.

The SHUV pigment gene (GenBank ID: JQ036217) was reverse transcribed from Siberian hamster retinal RNA (see Supporting Information). The WT, F86Y, S90A, and S90C SHUV genes (bovine rhodopsin numbering is used) were cloned into a tetracycline inducible pACMV-TetO vector after adding the 1D4 tag (the last 9 amino acids of bovine rhodopsin C-terminus, TETSQVAPA) to the genes' C-termini.[7,8] The WT and SHUV mutants were expressed in *GnTI*-HEK293S stable cell lines[9] and prepared under dim red light. Using established procedures[10,11] the pigments were regenerated with 11-*cis* retinal and purified via immunoaffinity chromatography in 0.02% n-dodecyl β-d-maltoside. The dark-state spectrum of WT SHUV revealed that this pigment has an absorption maximum ($\lambda_{max}$) at 359 nm (Fig. 2), consistent with the USB11 form.[12,13] Characterization of mutants reveals that S90A and S90C have almost identical spectra ($\lambda_{max}$ of 358 nm), whereas the F86Y mutant has a more prominent UV band (376 ± 2 nm) at pH 6.6, but a more prominent visible band (432 ± 3 nm) at pH 5.1 (Fig. 2). An acid denaturation assay showed that the absorption in the UV region is due to the dark-state species and not from free retinal resulting from protein instability (see Fig. S2 in Supporting Information).

A comparative analysis of the spectroscopic properties of the SHUV WT and mutants clearly suggest that the interactions

responsible for regulating the protonation state of the retinyl chromophore are preserved in S90A and S90C mutants, but significantly altered in the F86Y mutant. However, the nature of key electrostatic interactions and hydrogen bonding networks responsible for steering the mechanism of spectral tuning remain largely unexplored. Here, we analyze the SHUV ligand environment as described by structural models of WT and mutant SHUV pigments. The models are based on the X-ray structure of bovine rhodopsin (PDB code: 1U19)[14] (Fig. 1B) and are built by using density functional theory-quantum mechanics/molecular mechanics (DFT–QM/MM)[15] hybrid methods. The DFT–QM/MM models were optimized according to the ONIOM hybrid method[16] with electronic-embedding (EE) scheme,[17] as implemented in Gaussian09[18] and as described in our previous studies on rhodopsin.[19,20] Models for WT, S90A and S90C with USB linkages, are compared to models of the F86Y mutant with both USB and PSB linkages that account for the two distinct spectral features in the UV (~376 nm) and visible (~432 nm) regions (Fig. 2).

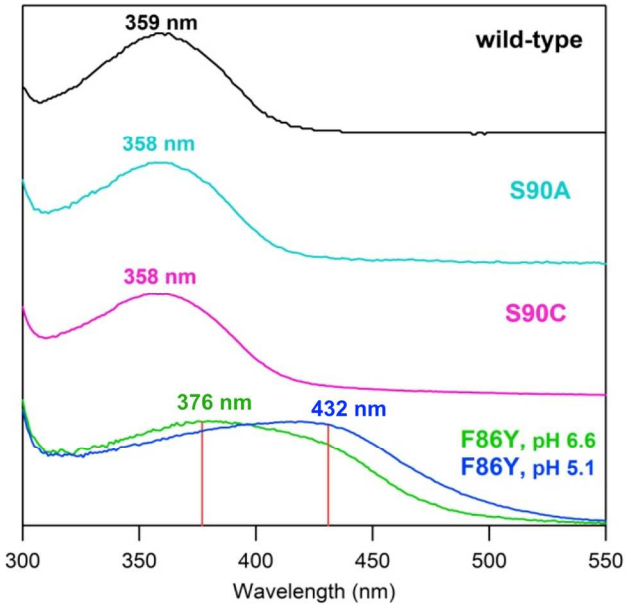


**Figure 2.** UV-Visible spectra of the WT, S90A, S90C and F86Y mutant SHUV pigments. The F86Y mutant exhibits two distinct peaks. In the case of F86Y mutant, the relative population of USB and PSB is deeply dependent on the pH as indicated. We used IgorPro's multipeak fitting function to deconvolute the F86Y spectrum into two Gaussian peaks with $\lambda_{max}$ (red lines) centered in the UV (376 ± 2 nm) and visible (432 ± 3 nm) regions.

***Wild-type:*** Although other pigments have higher homology with the SHUV (e.g., the human blue pigment with ~85% homology[22]), rhodopsin remains the most homologous pigment with a resolved X-ray crystal structure[14] including internal water molecules that are thought to be essential for functionality of visual pigments.[23,24] The DFT–QM/MM model of the SHUV pigment contains 26 water molecules that are also conserved in rhodopsin (Fig. 1B). Within 3.0 Å of the USB, there are 10 non-conserved residues present, including F86(M) and S90(G), with rhodopsin residues indicated in parentheses.[14] There are also 8 conserved key active site residues, including E113, E181, S186, C187, Y268 and Y192 that participate in forming an extended hydrogen bonding network (HBN) around the USB11 (see Supporting Information). T94 was also proposed to be part of this extended HBN in rhodopsin,[25] however, it is substituted by V94 in SHUV, a hydrophobic residue that disrupts the hydrogen bonding connectivity in the active site.

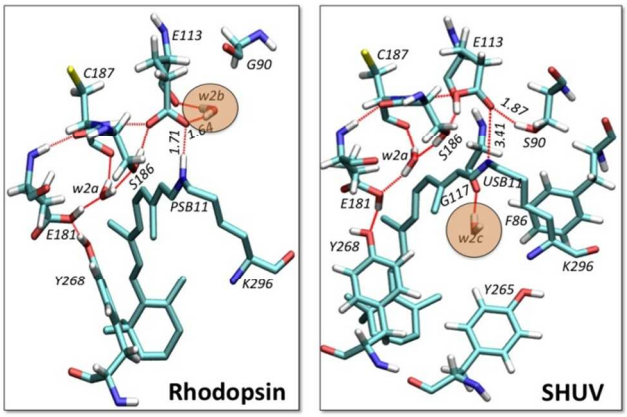


**Figure 3.** Comparison of the DFT-QM/MM optimized WT rhodopsin (left) and SHUV (right) pigments. Water molecules, w2b and w2c are highlighted by shaded orange circles. Amino acid numbers correspond to the rhodopsin primary sequence. Distances between the Schiff-base NH and E113 in rhodopsin and SHUV are indicated, in addition to the hydrogen bonding between w2b and E113 in rhodopsin and between S90 and E113 in SHUV.

In the DFT-QM/MM model of rhodopsin, an extended HBN is formed between Y268, E181, w2a, S186, C187, E113 and w2b (Fig. 3, left).[19,20] The protonated form of the chromophore is stabilized by hydrogen bonding with the negatively charged counterion E113 stabilized by w2b. However, with the USB11 in the SHUV pigment, the neutral (protonated) form of E113 is stabilized as a hydrogen bond donor to S186, which in turn becomes a hydrogen bond donor to E181 (Fig. 3, right). Internal water molecules are essential for the stability of HBNs in the active site,[23,24] including w2c near sites F86 and G117. Since the USB11 is shown to be stabilized by the protonated form of E113, which is also H-bonded to S90, we suggest that the presence of w2b near the SB is neither likely nor necessary to occur in the SHUV pigment (see Supporting Information).

***F86Y***: The UV-visible spectrum of the F86Y mutant exhibit two distinct peaks (~376 and ~432 nm), suggesting the coexistence of USB and PSB chromophores at equilibrium. The visible band was previously observed at 424 nm upon F86Y mutation in the mouse UV pigment, and was attributed to the presence of a PSB in the pigment.[22] In fact, isolation of the two species was reported to be difficult in the F86Y/E113Q double mutant due to pH dependent equilibrium,[22] also observed for the SHUV pigment although to a lesser extent. However, the molecular events underlying the transformation of USB11 to PSB11 upon F86Y mutation remained unexplored. We find that the F86Y mutation stabilizes hydrogen bonds that establish an *"inter-helical lock"* (IHL) between helices TM6, TM2 and TM3, with F86Y on TM2 functioning as a H-bond acceptor of Y265 in TM6, and as a H-bond donor to an internal water molecule (wat2c) that is H-bonded to the backbone of G117 on TM3 (Fig. 4). The IHL is aided by HBNs between the side chain and the backbone groups of amino acid residues Y265, F86Y, w2c, S118, E113, S90 and non-polar residues G117, A114, effectively establishing a strong contact between TM6, TM2 and TM3. Although Y268 is part of TM6, it is an hydrogen bond acceptor to E181 in the EII loop and therefore, is not as involved as Y265 in constrain-

ing the displacement of TM6. Displacement of the TM6 away from TM3 has been proposed to be a conformational change essential for the activation of rhodopsin and other GPCRs.[26-29] Comparison of the ONIOM QM/MM extrapolated energies reveal that F86Y mutant model with a PSB is more stable than with a USB by ~10 kcal/mol due to the presence of an IHL involving TM6, TM3 and TM2 helices (see section III of the Supporting Information).

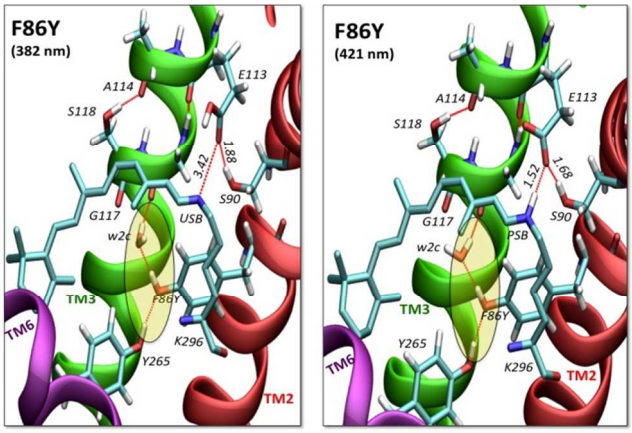


**Figure 4.** DFT-QM/MM models of the F86Y mutant with USB (left) and PSB (right) linkages, revealing an *inter-helical lock* (shaded region) between TM6 (purple), TM3 (green) and TM2 (red) by hydrogen-bonding (red dashed lines) of w2c and polar side-chains or backbone groups of amino acid residues Y265, F86Y, G117, S118, A114, E113 and S90.

***S90A, S90C***: Site 90 next to the USB in the SHUV pigment, involves the polar residue serine, which replaces the non-polar residue glycine at the equivalent site in rhodopsin. The side chain of S90 forms a weak H-bond with E113, establishing an interaction that is not possible in rhodopsin. This additional H-bond, however, displaces an internal water molecule (w2b in rhodopsin) to the position of w2c in SHUV (Fig. 3). To test the strength of key hydrogen bonds responsible for the IHL of the SHUV pigment, we have analyzed models of the S90A and S90C mutants. Upon S90A mutation, the HB between S90 and E113 as well as the inter-helical contact between TM2 and TM3 are lost, which induces an increase in distance between the USB and E113 compared to the WT (from 3.41→3.54 Å) (Fig. 5). In contrast, the S90C mutant induces smaller changes, with only slight stretching of the HB between S90 and E113 (from 1.87→1.89 Å). The stretching reflects weakening of the HB since the –SH group of cysteine is a poor donor, compared to the –OH group of serine. This increase in distance between the USB and E113 upon mutation of S90 is consistent with the unprotonated form of the SB in mammalian UV pigments.

The weaker H-bonding interactions, induced by C90 could lead to destabilization of the inter-helical contact between TM2 and TM3. Therefore, alterations in the HBN due to mutation of non-conserved residues at sites 86 and 90 may either prevent or promote the presence of a PSB in the active site. This is consistent with studies of avian SWS1 pigments ($\lambda_{max}$ = 390–440 nm) where a shift of the absorption $\lambda_{max}$, from violet to UV, is induced by the F86S and S90C mutations.[5,6,30] The F86S mutation is characteristic to avian violet pigments and an additional S90C mutation was assumed to cause deprotonation of the SB. It is thus plausible that the F86S mutation might induce formation of an IHL through HBNs as seen in the case of SHUV's F86Y mutant.

***Spectral tuning:*** To validate the QM/MM structural models through direct comparisons to experimental data, we have computed the absorption spectra of the QM/MM models by using *ab initio* multireference methods, including the spectroscopy oriented configuration interaction (SORCI+Q) method[31] with 6-31G(d) basis set and Amber96 level of theory[32], as implemented in the ORCA 2.6.19 program.[33] This methodology typically yields results in good agreement with experiments (within ±20 nm), as shown in our previous studies on related retinal proteins.[34]

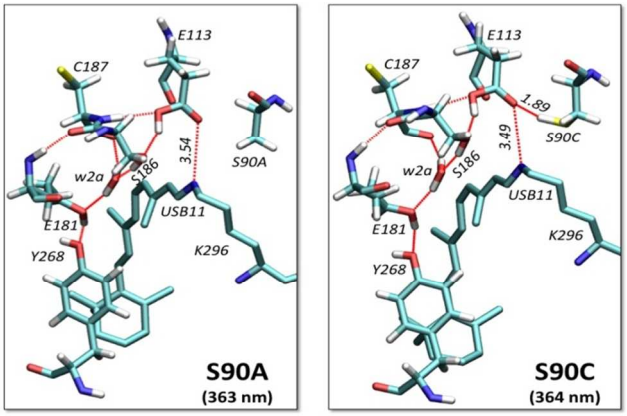


**Figure 5.** Comparison of the QM/MM optimized models of S90A (left) and S90C (right) SHUV mutants. HBNs comprised of S90, E113, S186, S187, w2a, E181 and Y268 residues are shown in red dashed lines. Distances between USB and E113 and between S90C and E113 are indicated in Å.

**Table 1.** Comparison of calculated and experimental absorption bands, including the wavelength of maximum absorption (λ) in nm, oscillator (*f*) and rotatory (*R*) strengths in au and the change in the ground- ($S_0$) and excited-state ($S_2$ for USB; $S_1$ for PSB) dipole moments (Δμ) of USB11 and/or PSB11 in the protein (QM/MM) environments of WT, F86Y, S90A and S90C SHUV pigment models. Strong, weak and broken HB refers to the nature of the hydrogen bond between S90 and E113. Numbers in superscript refer to the relative energies, whereas numbers in parentheses indicate the spectral shift relevant to the WT/USB11 model, except for F86Y/PSB11, which is referenced against F86Y/USB11.

| SHUV Pigment Models | First Vertical Excited State Properties | | | | |
|---|---|---|---|---|---|
| | Protein | | | | |
| | λ | *f* | *R* | Δμ | Expt. |
| $^{\text{Strong HB}}$WT/USB11 | 369 (0) | 1.62 | 0.13 | 11.26 | 359 (0) |
| F86Y/USB11$^{+10.392}$ | 382 (+13) | 1.23 | 0.10 | 10.00 | 376 (+17) |
| F86Y/PSB11$^{0.000}$ | 421 (+39) | 1.52 | 0.04 | 11.67 | 432 (+56) |
| $^{\text{Broken HB}}$S90A/USB11 | 363 (-6) | 0.35 | 0.00 | 5.18 | 358 (-1) |
| $^{\text{Weak HB}}$S90C/USB11 | 364 (-5) | 1.60 | 0.09 | 11.13 | 358 (-1) |

The comparison of calculated and experimental data reported in Table 1, shows very good agreement between the experimental absorption band and the calculated electronic vertical excitations, predicting that the WT model absorbs at 369 nm due to the presence of the USB and protonated E113 at the active site. Compared to the WT, both S90A and S90C pigments exhibit a blue shift of ~6 nm as S90A absorbs at 363 nm and S90C absorbs at 364 nm, respectively. The small blue shift can be attributed to the loss of and/or weakening of the HB[35] between sites 90 and 113, as mentioned in the previous

section discussing the S90A and S90C mutant spectra. In the case of the F86Y mutant, the QM/MM model with an USB absorbs at 382 nm, while the model with a PSB absorbs at 421 nm. The calculated values are in excellent agreement with the experimental measurements of ~376 and ~432 nm, respectively. Compared to the WT, the molecular origin of the spectral shifts can be traced back to the breaking (S90A) or weakening (S90C) of an intermolecular HB between S90 and E113 residues and to the formation of an HB involving the F86Y mutant (see Fig. S5 in the Supporting Information).

Another interesting finding revealed by our calculations is the excited state ($S_1/S_2$) level order reversal that correlates with the protonation state of the Schiff-base linkage (USB vs. PSB) and corresponding protonation state of the counterion at the chromophore binding site.[36] Also, the change in magnitude of the dipole moment ($\Delta\mu$) between the ground- and the excited-states and increase or decrease in the oscillator (*f*) and rotatory (*R*) strengths offers insight into the unique photophysical properties of the SHUV pigment. In this case, the dramatic decrease in *f* (from 1.62→0.35 au) and *R* (from 0.13→0.00 au) due to S90A mutation confirms the loss of a HB between S90 and E113 essential for stabilization of the counterion position. Similarly, the significant increase in *f* (from 1.23→1.52 au) and $\Delta\mu$ (from 10.00→11.67 D) values upon F86Y mutation correlates well with the increase in the number of dipolar sidechain groups in the active site that can enhance the dipole-protein charge interaction leading to a red (*opsin*) shift.[37]

In summary, we find that structural models of the WT and mutant SHUV pigments, validated through the analysis of their spectral properties and direct comparisons with experimental measurements, provide fundamental insights into the molecular origin of spectral tuning in ancestral photoreceptors. It is shown that formation of an *inter-helical lock* with specific amino acids, mediated by HBNs and internal water molecules, determines an arrangement of hydrogen bonds at the active site that stabilize the unprotonated form of the Schiff-base linkage and therefore the unique photophysical properties of the SHUV pigment. The structural factors governing the protonation state of the chromophore and therefore the spectral tuning mechanism, involve not only amino acid residues in direct contact with the ligand, but also an extended network of hydrogen bonds establishing an *inter-helical lock* mechanism.

## SUPPORTING INFORMATION

The supporting information contains the primary sequence alignment between SHUV and rhodopsin, experimental and computational details of the system set-up. This information is available free of charge via the Internet at http://pubs.acs.org

## ACKNOWLEDGMENTS

V.S.B acknowledges supercomputer time from NERSC and support from the National Science Foundation (NSF) grant CHE-0911520. E.C.Y.Y. acknowledges funding. Additional support was provided by a NSF fellowship DGE-0644492 to V.L.M. and by a NSF Career Grant MCB-0955407 to E.C.Y.Y.

### Corresponding Authors

sivakumar.sekharan@yale.edu; elsa.yan@yale.edu; victor.batista@yale.edu

## REFERENCES

(1) Yokoyama, S. *Annu. Rev. Genomics Hum. Genet.* **2008**, *9*, 259.
(2) Bowmaker, J. K. *Vis. Res.* **2008**, *48*, 2022.
(3) Shichida, Y.; Matsuyama, T. *Philos. Trans. R. Soc. Lond. B. Biol. Sci.* ***2009***, *364*, 2881.
(4) Hunt, D. M.; Carvalho, L. S.; Cowing, J. A.; Davies, W. L. *Philos. Trans. R. Soc. Lond. B. Biol. Sci.* **2009**, *364*, 2941.
(5) Shi, Y.; Radlwimmer, B.; Yokoyama, S. *Proc. Acad. Natl. Sci. U.S.A.* **2001**, *98*, 11731.
(6) Shi, Y.;Yokoyama, S. *Proc. Acad. Natl. Sci. U.S.A.* **2003**, *100*, 8308.
(7) Chang, B. S. W.; Kazmi, M. A.; Sakmar, T. P. *Methods Enzymol.* **2002**, *343*, 274.
(8) Reeves, P. J.; Kim, J. M.; Khorana, H. G. *Proc. Acad. Natl. Sci. U.S.A.* **2002**, *99*, 13413.
(9) Reeves, P. J.; Callewaert, N.; Contreras, R.; Khorana, H. G. *Proc. Acad. Natl. Sci. U.S.A.* **2002**, *99*, 13419.
(10) Oprian, D. D.; Molday, R. S.; Kaufman, R. J.; Khorana, H. G. *Proc. Acad. Natl. Sci. U.S.A.* **1987**, *84*, 8874.
(11) Chan, T.; Lee, M.; Sakmar, T. P. *J. Biol. Chem.* **1992**, *267*, 9478.
(12) Vought, B.W.; Dukkipatti, A.; Max, M.; Knox, B.E.; Birge, R.R. *Biochemistry* **1999,** *38*, 11287.
(13) Mooney, V. L.; Szundi, I.; Lewis, J. W.; Yan, E. C. Y.; Kliger, D. S. *Biochemistry* **2012**, *51*, 2630.
(14) Okada, T.; Sugihara, M.; Bondar, A.N.; Elstner, M.; Entel, P. Buss, V. *J. Mol. Biol.* **2004**, *342*, 571.
(15) Warshel, A.; Levitt, M. *J. Mol. Biol.* **1976**, *103*, 227.
(16) Vreven,T.; Morokuma, K.; Farkas, O.; Schlegel, H. B.; Frisch, M. J. *J. Comput. Chem.* **2003**, *24*, 760.
(17) Bakowies, D.; Thiel, W. *J. Phys. Chem.* **1996**, *100*, 10580.
(18) Frisch, M. J.; et al. *Gaussian 09,* Revision A.02; Gaussian, Inc.: Wallingford, CT, 2009.
(19) Gascón, J. A.; Batista, V. S. *Biophys. J.* **2004**, *87*, 2931.
(20) Gascón, J. A.; Sproviero, E. M.; Batista, V. S. *J. Chem. Theory Comput.* **2005**, *1*, 674.
(21) Larkin, M. A.; *Blackshields, G.; Brown N. P.; Chenna, R.; McGettigan, P. A.; McWilliam, H.; Valentin, F.; Wallace, I. M.; Wilm, A.;* Lopez, R.; Thompson, J. D.; Gibson, T. J.; Higgins, D. G. Clustal W and Clustal X version 2.0. *Bioinformatics* **2007**, *23*, 2947.
(22) Fasick, J. L.; Applebury, M. L.; Oprian, D. D. *Biochemistry* **2002**, *41*, 6860.
(23) Okada, T.; Fujiyoshi, Y.; Silow, M.; Navarro, J.; Landau, E. M.; Shichida, Y. *Proc. Natl. Acad. Sci. USA* **2002**, *99*, 5982.
(24) Katayama, K.; Furutani, Y.; Imai, H.; Kandori, K. *Angew. Chem. Int. Ed.* **2010**, *49*, 891.
(25) Sugihara, M.; Buss, V.; Entel, P.; Hafner, J. *J. Phys. Chem. B.* **2004**, *108*, 3673.
(26) Farrens, D. L.; Altenbach, C.; Yang, K.; Hubbell, W. L.; Khorana, H. G. *Science* **1996**, *274*, 768.
(27) Sheikh, S. P.; Zvyaga, T. A.; Lichtarge, O.; Sakmar, T. P.; Bourne, H. R. *Nature* **1996**, *383*, 347.
(28) Hubbell, W. L.; Altenbach, C.; Hubbell, C. M.; Khorana, H. G. *Adv. Protein. Chem.* **2003**, *63*, 243.
(29) Altenbach, C.; Kusnetzow, A. K.; Ernst, O. P.; Hofmann, K. P.; Hubbell, W. L.; *Proc. Natl. Acad. Sci. U.S.A.* **2008**, *105*, 7439.
(30) Bowmaker, J. K.; Heath, L. A.; Wilkie, S. E.; Hunt, D. M. *Vis. Res.* **1997**, *37*, 2183.
(31) Neese, F. A. *J. Chem. Phys.* **2003**, *119*, 9428.
(32) Cornell, W. D. *et al*. A. *J. Am. Chem. Soc.* **1995**, *117*, 5179.
(33) Neese, F. *ORCA-an ab initio, DFT and semiempirical electronic structure package*, v. 2.6. **2007.**
(34) (a) Sekharan, S.; Altun. A.; Morokuma, K. *J. Am. Chem. Soc.* **2010**, *132*, 15856. (b) Sekharan, S.; Morokuma, K. *J. Am. Chem. Soc.* **2011**, *133*, 4734. (c) Sekharan, S.; Morokuma, K. *J. Am. Chem. Soc.* **2011**, *133*, 19052. (d) Sekharan, S.; Katayama, K.; Kandori, H.; Morokuma, K. *J. Am. Chem. Soc.* **2012**, *134*, 10706. (e) Sekharan, S.; Wei, J. N; Batista, V. S. *J. Am. Chem. Soc.* **2012**, *134*, 19536. (f) Pal, R.; Sekharan, S.; Batista, V. S. *J. Am. Chem. Soc.* **2013**, *135*, 9624.
(35) a) Zhao, G. J.; Liu, J. Y.; Zhou, L. C.; Han, K. L. *J. Phys. Chem. B.* **2007**, *111*, 8940. b) Zhao, G. J.; Han, K. L. *Biophys, J.* **2008**, *94*, 38. c) Zhao, G. J.; Han, K. L. *Acc. Chem. Res.* **2012**, *45*, 404.
(36) Birge, R. R.; Murray, L. P.; Pierce, B. M.; Akita, H.; Balogh-Nair, V.; Findsen, L. A.; Nakanishi, K. *Proc. Natl. Acad. Sci. U.S.A* **1985**, *82*, 4117.
(37) Mathies, R.; Stryer, L. *Proc. Natl. Acad. Sci. U.S.A.* **1976**, *73*, 2169.

## TOC Figure

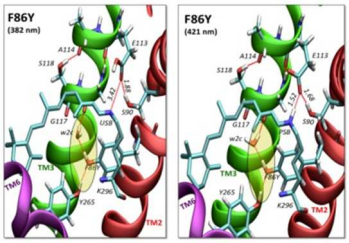
F86Y
(382 nm)
A114
S118
E113
L125
T126
S90
G117
w2c
GSB
TM3
F86
K296
Y265
TM2
F86Y
(421 nm)
A114
S118
E113
L125
T126
S90
G117
w2c
GSB
TM3
F86
Y265
K296
TM2

# Supporting Information

*for*

# Spectral Tuning of Ultraviolet Cone Pigments: An Interhelical Lock Mechanism

Sivakumar Sekharan[†*], Victoria L. Mooney[†], Ivan Rivalta[†], Manija A. Kazmi[‡], Maureen Neitz[§], Jay Neitz[§], Thomas P. Sakmar[‡], Elsa C. Y. Yan[†*], Victor S. Batista[†,*]

[†]Department of Chemistry, Yale University, P.O. Box 208107, New Haven, CT 06520-8107
[†]Laboratory of Chemical Biology and Signal Transduction, Rockefeller University, New York, NY 10065
[§]School of Medicine, Department of Ophthalmology, University of Washington, Seattle, WA 98195

***Total Number of Pages: S12***

***Table of Contents***

# I. Experimental Section

***Nucleic acid extraction, polymerase chain reaction, and DNA sequencing:*** Nucleic acids were extracted by mincing tissue from *Phodopus sungorus* liver or retina and placing it in 200 µl of 10 mM Tris-HCl, pH 8.0, 0.1 mM EDTA, pH 8.0, 1% (w/v) sodium dodecyl sulfate, and 4 mg/ml proteinase K. The mixture was incubated for 8-12 hours at 55 °C. Samples were then extracted with phenol and chloroform, followed by nucleic acid precipitation from ethanol.[1] The *P. sungorus* retinal RNA was reverse transcribed (ABI), resulting in two separate, overlapping segments of the UV pigment cDNA. Both segments were amplified and sequenced. *P. Sungorus* liver nucleic acid was used directly in the PCR reaction to amplify a segment extending from exon 4 into exon 5, which included intron 4. A Kozak sequence and KpnI site were inserted at the 5' end of the UV pigment gene (GenBank ID: JQ036217).[2,3] To the 3' end of the SHUV gene, a 1D4 tag (the last 9 a.a. of the bovine rhodopsin C-terminus, TETSQVAPA) was added and a NotI restriction site was inserted immediately following the stop codon. The UV pigment gene was then cloned into the tetracycline inducible pACMV-TetO vector.[4,5] DNA sequencing was used to confirm the final sequence of the pACMV-TetO-UV plasmid. The UV gene contained the silent mutations Q233Q (CAA → CAG) and A310A (GCC → GCA). F86Y, S90A, and S90C SHUV mutants were prepared via point mutations.

***Protein expression & purification:*** *GnTI-* HEK293S cells were transfected with the pACMV-TetO-UV plasmid using lipofectamine (Invitrogen). The UV stable cell line was made as previously reported.[6] UV pigment expression was induced upon addition of 5 mM sodium butyrate and 2 µg/mL tetracycline; cells were harvested 48 hr after induction.[4] The protein was prepared under dim red light, using procedures reported previously.[2,7] The cells were washed with Buffer A (50 mM HEPES, pH 6.6; 140 mM NaCl, 3 mM MgCl2) before being regenerated overnight in Buffer B (5 µg/mL each of aprotinin and leupeptin and 7.15 µM 11-*cis* retinal in Buffer A) at 4°C. After centrifugation, the cell pellet was resuspended in solubilization buffer

(1% w/v n-dodecyl-β-D-maltoside (DM), 20% w/v glycerol, and 0.1 mM phenylmethanesulfonyl fluoride in 75% v/v buffer A) for ~5 hr. Immunoaffinity chromatography was used to purify the SHUV pigment[2,8,9], wherein the 1D4 epitope cloned into the C-terminus of the UV pigment was recognized by the 1D4 monoclonal antibody bound to agarose resin. The resin was washed thrice with Buffer C (47 mM HEPES, pH 6.6; 132 mM NaCl, 2.8 mM $MgCl_2$, 0.02% DM, and 7.5% w/v glycerol). The UV pigment was eluted into Buffer C upon addition of 0.726 mg/mL 1D5.

***Pigment characterization:*** After purification of the SHUV pigment and its mutants, UV-visible spectra were collected to ensure that their dark states were functional. To produce the photoproducts, the UV pigment was illuminated for 60 s with 365-nm light. This resulted in a shift in the pigments' $\lambda_{max}$s to ~379 nm, consistent with the photoconversion of retinal from an 11-*cis* to all-*trans* isomer and the formation of an active Meta II-like product. The extinction coefficient for dark-state, wild-type SHUV was determined using an acid denaturation assay.[10] Addition of hydrochloric acid to the dark-state pigment caused a red shift from 359 nm to 440 nm, consistent with the formation of a protonated Schiff base linkage between the denatured opsin and the retinylidene chromophore (Fig. S1). From three separate trials, a value of 43,300 ± 700 $M^{-1}$ $cm^{-1}$ was calculated for the 359 nm extinction coefficient of the dark-state UV pigment using the known $\varepsilon_{440}$ of 30,800 $M^{-1}cm^{-1}$ for a protonated Schiff base in solution. A spectral ratio ($A_{280}/A_{359}$) of 2.1 was calculated for the dark-state SHUV. This acid denaturation technique was also used for the F86Y mutant to determine whether that 376 nm UV peak present in the pigment's dark-state is due to free retinal. After pigment denaturation, the 376 nm and 432 nm peaks both shifted to ~440 nm, indicating the presence of an intact Schiff base for both species (Fig. S2). All UV-visible spectroscopy was carried out in an UV-2450 Shimadzu spectrophotometer.

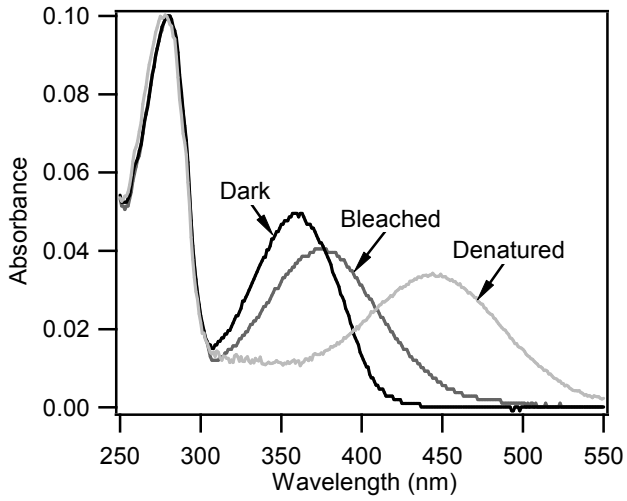


***Figure S1.*** *UV-Visible spectra of the wild-type Siberian hamster UV pigment before (Dark, 359 nm) and after (Bleached, 379 nm) being bleached for 1 min with 365 nm light. The dark-state SHUV was acid denatured (440 nm) in order to determine the extinction coefficient of the dark-state peak at 359 nm.*

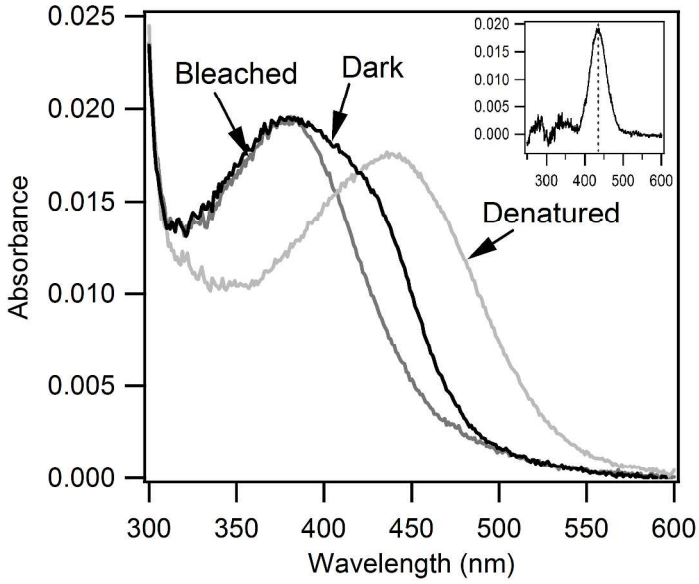


***Figure S2.*** *UV-Visible spectra of the Siberian hamster UV pigment F86Y mutant. In all three spectra, the absorbance was normalized to 0.1 at 280 nm. In the dark-state, there are two species present, one absorbing in the UV and the other in the visible region (Dark). Upon photoactivation with white light for 10 min, the* $\lambda_{max}$ *shifts to 380 nm (Bleached). The dark-state pigment was also acid denatured to ensure that the UV peak in the dark-state was not due to retinal that had hydrolyzed from the pigment. The inset shows the dark minus bleached difference spectrum with a vertical line is centered at 435 nm.*

## II. Computational Details

***Primary sequence and secondary structure of the SHUV pigment:*** We developed a molecular model of the dark-state SHUV pigment to gain a better understanding of the role of counterion (E113), water molecules and H-bonding networks in the active site. Alignment of the primary sequences of SHUV pigment and bovine rhodopsin using the clustalW revealed that there is 43% identity between the two sequences and 193 non-conserved amino acid residues. We used the crystal structure of rhodopsin (PDB code: 1U19 at 2.2 Å resolution)[11] as template to create the homology model of the SHUV pigment (Fig. S3A, S3B). Nonconserved residues have been mutated using the standard mutation procedure implemented in the Schrödinger's Maestro suite[13] (the standard mutate.py script uses the standard Maestro rotamer libraries) and after each mutation the overall structure was relaxed by using the impref Maestro utility. Protonation states of all titratable residues are assigned based on PROPKA $pK_a$ calculations[14] and visual inspection. Geometry minimizations were based on the impact molecular mechanics engine[15] using the OPLS_2005 force field[16,17] (Fig. S3C) and setting the maximum RMSD to 0.30 Å. No simulated annealing/molecular dynamics refinement was carried out because the proposed homology model was simply used as an initial structure for the QM/MM refinement. The RMSD cutoff is to ensure a minimal movement of the system with respect to the initial Rhodopsin template during the preliminary MM refinement (i.e. the impref optimization), which is aimed at removing close contacts at the mutation sites. The disulfide bond between Cys110 in transmembrane helix 3 and Cys187 in extracellular loop 2 (EL2) was maintained in the homology model.

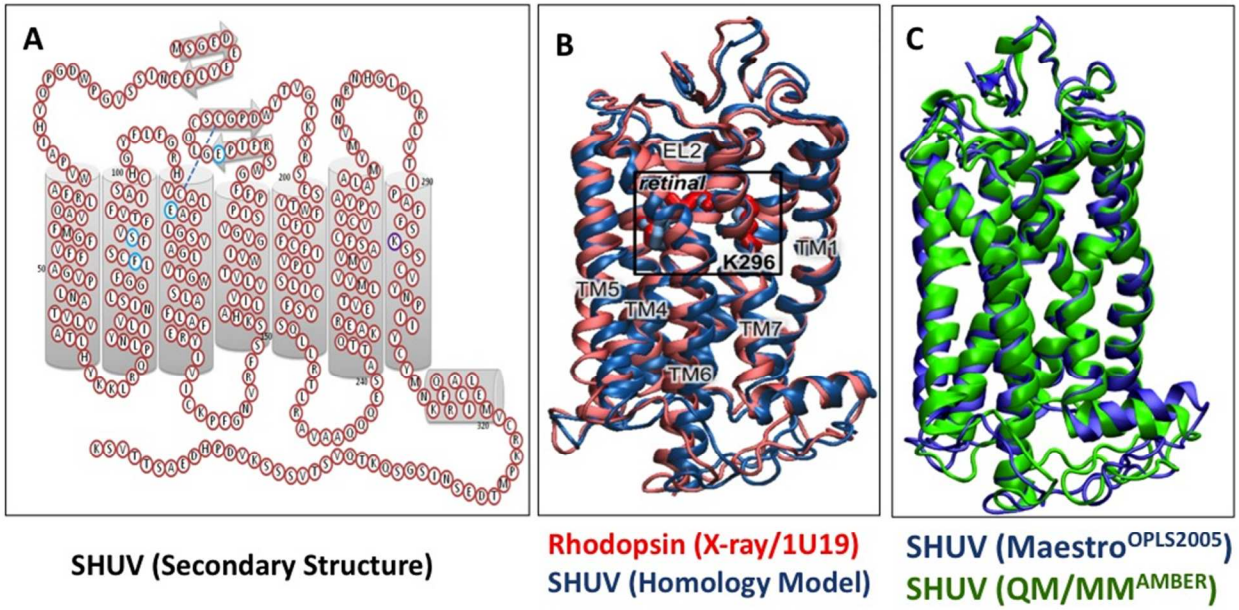


***Figure S3.*** *(A) The numbering system used in the secondary structure of the Siberian hamster UV (SHUV) pigment correspond to that of rhodopsin; there is a 5-residue shift in the N-terminus such that from H1-H8, rhodopsin residue numbers are 5 greater than those of UV residues. The dashed line connecting C110 to C187 represents a disulfide bond. The purple circle surrounds K296, the lysine to which 11-cis retinal binds. Residues that are in blue circles are known to interact with the Schiff base (E113 and E181) or are important for spectral tuning (F86 and S90) in vertebrate visual pigments. (B) Superposition of the X-ray structure of bovine rhodopsin (red) with Maestro-MM optimized starting structure of the SHUV homology model (blue). The pigments are orientated such that the extracellular side is above and the cytoplasmic side is below the transmembrane region. The secondary structure elements (cartoon), including the transmembrane helices (TM) and extra-cellular loop 2 (EL2), as well as the K269 and 11-cis-retinyl chromophore (sticks) are shown. (C) Superposition of the Maestro MM (OPLS2005) optimized starting structure (blue) with the ONIOM QM/MM (Amber) optimized fully relaxed homology model of the SHUV pigment. The positions of the seven TM α-helices are shown to be very well conserved during the geometry optimizations and the overall RMSD of the fully optimized QM/MM structure with respect to Maestro optimized starting structure is 1.46 Å.*

***Chromophore Binding Pocket:*** Within 3 Å of the chromophore in dark-state SHUV there are 10 non-conserved residues present, including F86(M) and S90(G), where rhodopsin residues are indicated in parentheses (Fig. S4). There are also 8 key active site residues that are conserved, including E113, E181, and Y268. Amino acid residues Y192 and T94 have been proposed to be also part of the extended hydrogen-bonding network in rhodopsin. While amino acid residue Y192 is conserved in the SHUV pigment, the hydrophobic residue V94 substitutes the polar residue T94, disrupting one of the possible hydrogen bonds for the E113 counterion. On the other hand, the rhodopsin non-polar residue G90 is substituted in the SHUV pigment by the polar residue S90, which can establish a hydrogen-bond interaction with the close E113 side chain.

Therefore, the SHUV pigment and rhodopsin hydrogen-bonding networks near E113 are expected to be significantly different.

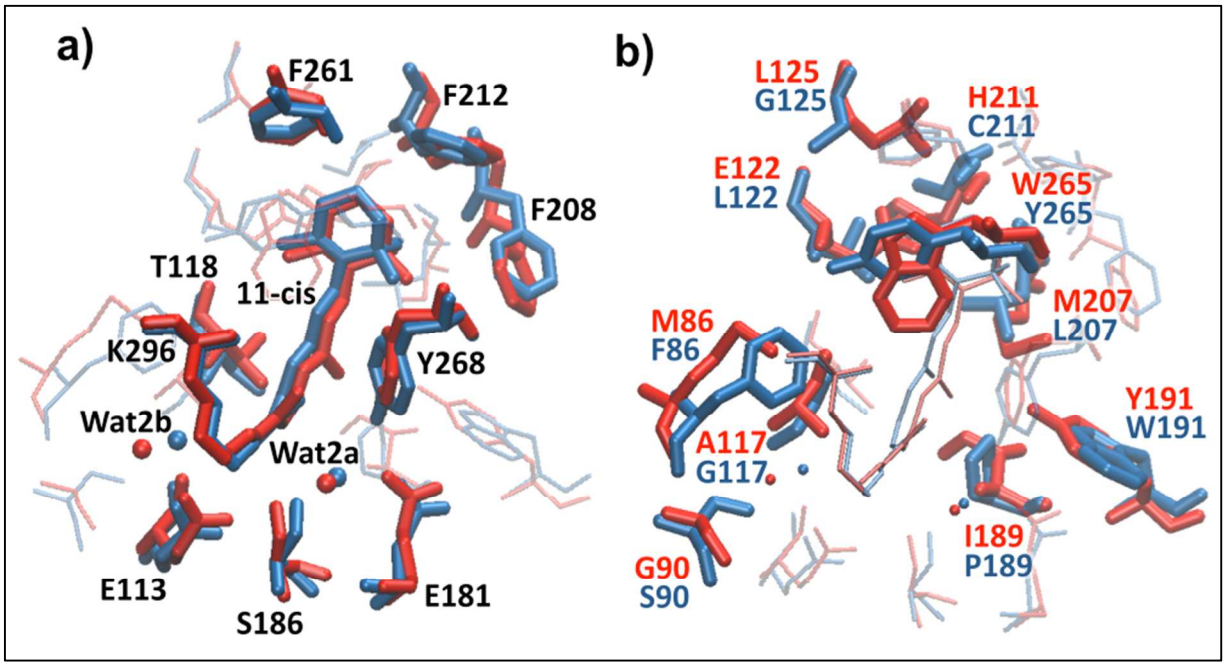


***Figure S4.*** *Superposition of the retinal binding pockets of bovine rhodopsin (red) and the SHUV pigment homology model (blue) after alignment of α-carbon atoms of amino acid residues within 3 Å of the bound retinal. Oxygen atoms belonging to water molecules (w2a and w2b) in the binding pockets are shown as spheres. a) Identity elements conserved among the two pigment types (including the water molecules) in the retinal binding pockets are highlighted, as well as the 11-cis retinal/K296 Schiff bases. b) Non-conserved amino acid residues in the binding pockets are highlighted.*

***MM and Hybrid QM/MM Calculations:*** The pre-refined homology model obtained using the Maestro suite was used as a starting structure to perform a series of initial pure AMBER geometry optimizations to remove close contacts and find more optimum positions for flexible groups in the entire protein. All MM calculations in the ensuing the QM/MM calculations were performed with AMBER96 force field and TIP3P water model. A series of initial pure AMBER geometry optimizations was performed to remove close contacts and find more optimum positions for flexible groups in the protein: (i) First, only the long flexible chains at the C and N terminals of the protein were optimized. (ii) Second, the flexible chains and water molecules in the protein were optimized. (iii) Finally, the full protein was optimized without any constraints. The resulting coordinates were fully optimized with a hybrid QM/MM (QM=B3LYP/6-31G*; MM=AMBER) method in ONIOM (Our own *N*-layer Integrated molecular Orbital + molecular Mechanics)[18] using electronic embedding scheme[19], which incorporates the partial charges of the

MM region into the quantum mechanical Hamiltonian. This technique provides a better description of the electrostatic interaction between the QM and MM regions (as it is treated at the QM level) and allows the QM wavefunction to be polarized as described in our previous works on rhodopsin.[20-24] The positions of the seven α–helices were very well conserved during the geometry optimizations. The QM model part includes full unprotonated or protonated Schiff base of 11-*cis*-retinyl chromophore (USB11 for WT, F86Y, S90A, S90C models and PSB11 for F86Y) with side-chain N–H moiety of Lys296 along with a hydrogen link atom[25] at the QM/MM boundary plus full E113 counterion residue in the protonated (when USB11 is present) and in unprotonated forms (when PSB11 is present). All single-point *ab initio* QM/MM calculations on the resulting coordinates were carried out with the ORCA 2.6.19 program package.[26] We applied three-root spectroscopy oriented configuration interaction (SORCI) method with Davidson correction (+Q) for excitations higher than doubles on complete active space self-consistent field (CASSCF) wave functions to calculate absorption and circular dichroism (CD) spectra. All multireference (MR) *ab initio* calculations were carried out using the 6-31G* basis set[27-30] plus an auxiliary basis set (SV/C)[31-33] to speed-up the calculations. The active space encompasses 6 electrons in 6 orbitals. Computational efficiencies of SORCI+Q calculations were enhanced by setting $T_{pre}$, $T_{nat}$ and $T_{sel}$ thresholds to $10^{-4}$, $10^{-6}$ and $10^{-6}$ *E*h, respectively.[34-38] The core orbitals with energies of less than -4 $E_h$ were frozen and a level shift of 0.4 $E_h$ was applied in all perturbative treatments.

# III. Energetics

**Table S1:** The energy values presented in Table S1 correspond to the calculated ONIOM QM/MM extrapolated energies and it shows that the USB form is more stable in the WT, S90A and S90C models, whereas the PSB form is more stable in the F86Y model. The findings are attributed to the absence or presence of an Inter-Helical Lock (IHL) involving TM6—TM2—TM3 helices in the active site.

| ***SHUV Models*** | ***ONIOM QM/MM Extrapolated Energy (kcal.mol$^{-1}$)*** | | ***Inter-Helical Lock between TM6—TM2—TM3*** |
|---|---|---|---|
| | ***USB*** | ***PSB*** | |
| *WT* | *0.000* | *+6.780* | *Absent* |

| | | | |
|---|---|---|---|
| *S90A* | *0.000* | *+4.687* | *Absent* |
| *S90C* | *0.000* | *+5.838* | *Absent* |
| *F86Y* | *+10.392* | *0.000* | *Present* |

## IV. Comparative analysis of w2c position in the active site.

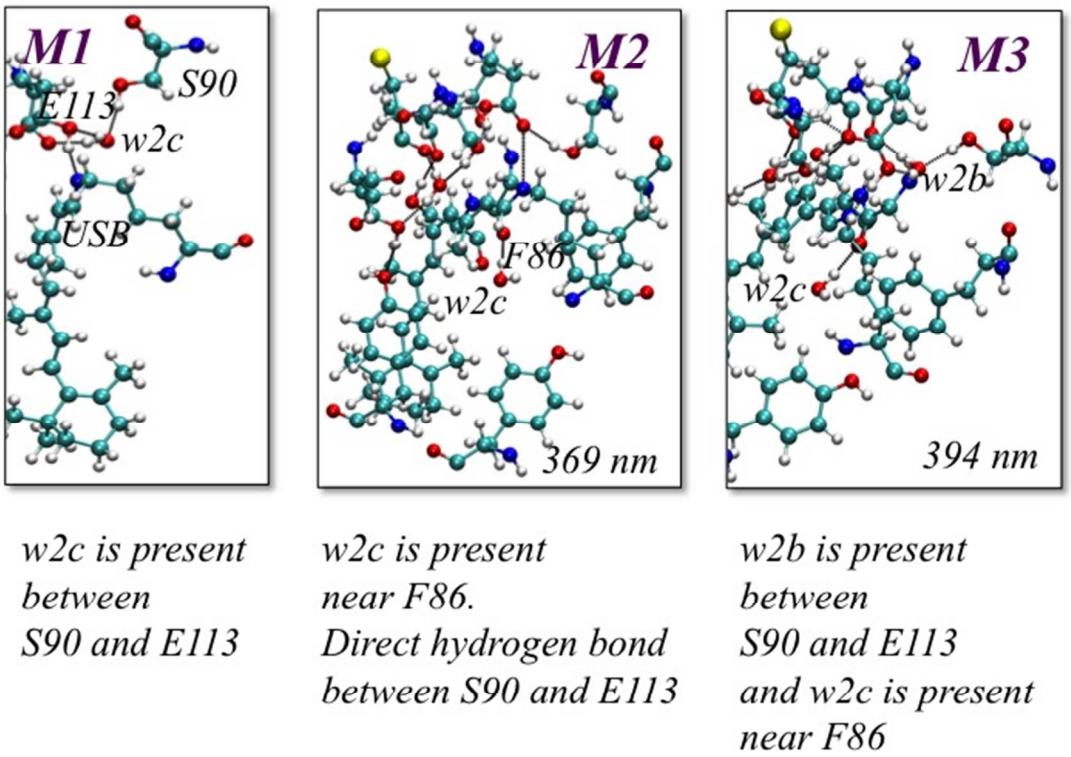


***Figure S5***. *QM/MM analysis of three different SHUV models (M1, M2, M3) that differs in the position of w2c in the active site. In the case of M1, w2c is present between S90 and E113 and occupies the position corresponding to w2b in rhodopsin. In the case of M2, w2c is present near F86 and as a result, there is a direct hydrogen bond between S90 and E113. Comparison of the ONIOM extrapolated energies reveal that, M1 is energetically unstable by more than 15 kcal/mol compared to M2. In the case of M3, the active site involves both w2b and w2c water molecules (w2b between S90 and E113 and w2c near F86) and the calculated* $\lambda_{max}$ *is red shifted by almost 40 nm compared to the experimental value (359 nm). Therefore, we rule out M1 and M3 models as possible wildtype structural models for the SHUV pigment.*

## V. Correlation between the intermolecular hydrogen bonding networks and frontier molecular orbital analysis of the electronic transition responsible for the spectral blue shift in the SHUV mutant (S90A, S90C) models.

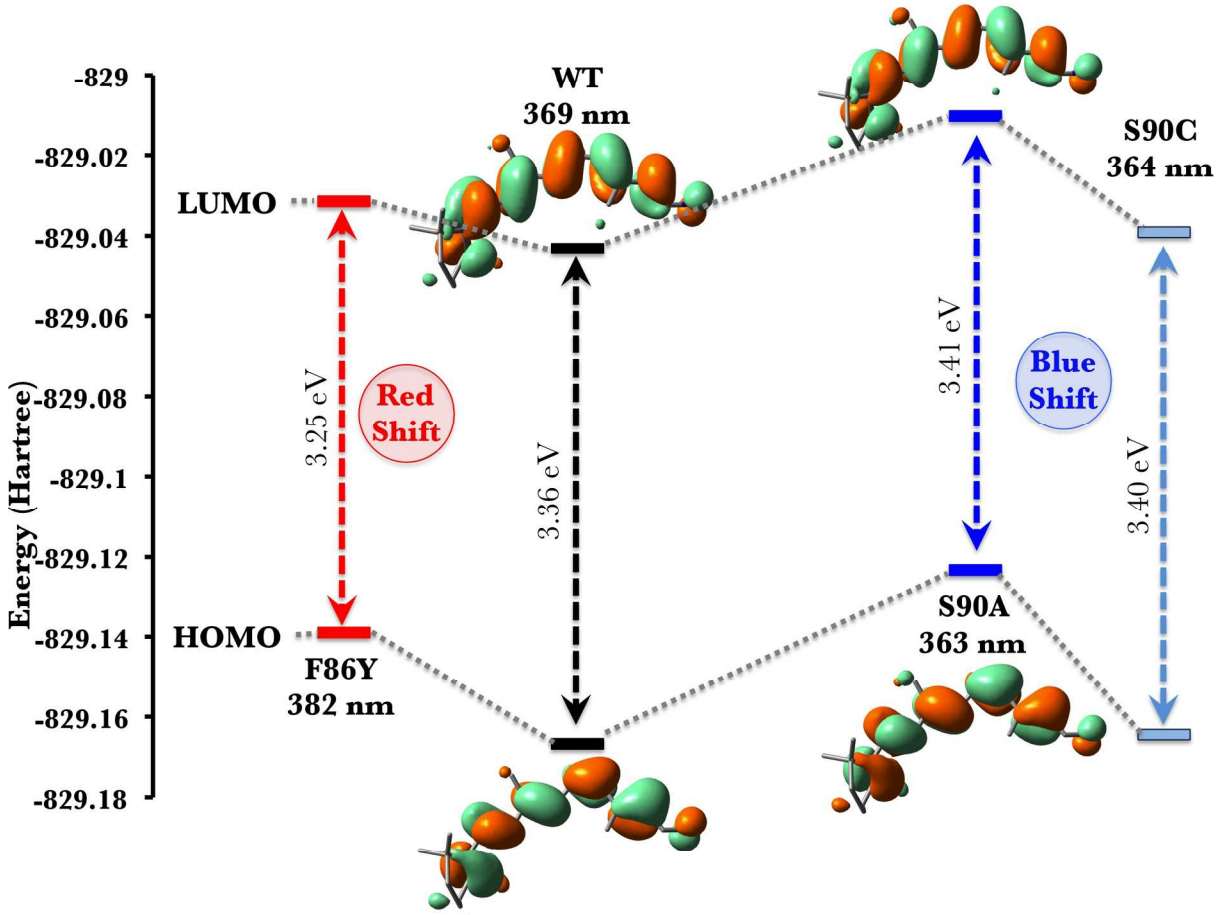


***Figure S6***. *The analysis shows that breaking or weakening of the hydrogen bond (between S90 and E113 residues) due to S90A and S90C mutations increases the energy gap and induces a spectral blue shift of ~6 nm, whereas formation of a hydrogen bond involving F86Y mutant decreases the energy gap and induces a spectral red shift of 13 nm relative to the WT.*

# VI. References


1. Cobb, J. K.; Bialozynski, C.; Neitz, J.; Jacobs, G. H.; Neitz, M. *Invest. Ophthalmol. Vis. Sci.* **1999**, *40*, S353
2. Oprian, D. D.; Molday, R. S.; Kaufman, R. J.; Khorana, H. G. *Proc. Acad. Natl. Sci. U.S.A.* **1987**, *84*, 8874.
3. Kozak, M. *Nucleic Acids Res.* **1984**, *12*, 857.
4. Reeves, P. J.; Kim, J. M.; Khorana, H. G. *Proc. Acad. Natl. Sci. U.S.A.* **2002**, *99*, 13413.
5. Chang, B. S. W.; Kazmi, M. A.; Sakmar, T. P. *Methods Enzymol*. **2002**; *343*, 274.
6. Yan, E. C. Y.; Epps, J.; Lewis, J. W.; Szundi, I.; Bhagat, A.; Sakmar, T. P.; Kliger, D. S. *J. Phys. Chem. C* **2007**, *111*, 8843.
7. Babu, K. R.; Dukkipati, A.; Birge, R. R.; Knox, B. E. *Biochemistry* **2001**, *40*, 13760.
8. Franke, R. R.; Sakmar, T. P.; Graham, R. M.; Khorana, H. G. *J. Biol. Chem.* **1992**, *267*, 14767.
9. Chan, T.; Lee, M.; Sakmar, T. P. *J. Biol. Chem.* **1992**, *267*, 9478.
10. Kito, Y.; Suzuki, T.; Azuma, M.; Sekoguti, Y. *Nature* **1968**, *218*, 955.
11. Okada, T.; Sugihara, M.; Bondar, A.N.; Elstner, M.; Entel, P. Buss, V. *J. Mol. Biol.* **2004**, *342*, 571.
12. Combet, C.; Blanchet, C.; Geourjon C, Deleage, G. *Trends in Biochem. Sci.* 2000, 147-150.
13. Maestro, version 9.0, Schrödinger, LLC, New York, NY, 2009.
14. Li, H.; Robertson, A. D.; Jensen, J. H. *Proteins: Struct. Funct. Bioinf.* ***2005****, 61*, 704.
15. Banks, J.; Beard, H. S.; Cao, Y. X.; Cho, A. E.; Damm, W.; Farid, R.; Felts, A. K.; Halgren, T. A.; Mainz, D. T.; Maple, J. R.; Murphy, R.; Philipp, D. M.; Repasky, M. P.; Zhang, L. Y.; Berne, B. J.; Friesner, R. A.; Gallicchio, E.; Levy, R. M. *J. Comp. Chem.* **2005**, 1752.
16. Jorgensen, W. L.; Maxwell, D. S.; TiradoRives, J. *J. Am. Chem. Soc.* **1996**, *118*, 11225.
17. Kaminski, G. A.; Friesner, R. A.; Tirado-Rives J, Jorgensen, W. L. *J. Phys. Chem.* **2001**, *105*, 6474.
18. Vreven, T.; Morokuma, K. *Ann. Rep. Comp. Chem.* **2006**, *2*, 35.
19. Antes, I.; Thiel, W. Hybrid Quantum Mechanical and Molecular Mechanical Methods; Gao, J., Ed.; ACS Symposium Series 712, American Chemical Society; Washington DC, **1998**; pp 50-65.
20. Gascón, J. A.; Batista, V.S. *Biophys. J.* **2004**, *87*, 2931.
21. Gascón, J. A.; Sproviero, E.M.; Batista, V. S. *J. Chem. Theory Comput.* **2005**, *1*, 674.
22. Gascón, J. A.; Sproviero, E.M.; Batista, V. S. *Acc. Chem. Res.* **2006**, *39*, 184.
23. Sekharan, S.; Wei, J. N; Batista, V. S. *J. Am. Chem. Soc.* **2012**, *134*, 19536.
24. Pal, R.; Sekharan, S.; Batista, V. S. *J. Am. Chem. Soc.* **2013**, *135*, 9624.
25. Bakowies, D.; Thiel, W. *J. Phys. Chem.* **1996**, *100*, 10580.
26. Neese F, (2007) *ORCA-an ab initio, DFT and semiempirical electronic structure package*, version 2.6, revision 19; Institut für Physikalische und Theoretische Chemie,

Universita¨t Bonn, Germany, 2007. Latest version available from http://www.thch.uni-bonn.de/tc/orca
27. Ditchfield, R.; Hehre, W. J.; Pople, J. A. *J. Chem. Phys.* **1971**, *54*, 724–728.
28. Hehre, W. J.; Ditchfield, R.; Pople, J. A. *J. Chem. Phys.* **1972**, *56*, 2257–2261.
29. Hariharan, P. C.; Pople, J. A. *Theor. Chim. Acta* **1973**, *28*, 213–222.
30. Clark, T.; Chandrasekhar, J.; Spitznagel, G. W.; Schleyer, P. v. R. J. Comput. Chem. **1983**, *4*, 294–301.
31. The SV/C auxiliary basis set was obtained from the TURBOMOLE basis set library under ftp.chemie.uni-karlsruhe.de/pub/cbasen.
32. Eichkorn, K.; Weigend, F.; Treutler, O.; Ahlrichs, R. *Theor. Chem. Acc.* **1997**, *97*, 119–124.
33. Weigend, F.; Häser, M. *Theor. Chem. Acc.* **1997**, *97*, 331–340.
34. Neese, F. *J. Chem. Phys.* **2003**, *119*, 9428–9443.
35. Wanko, M.; Hoffmann, M.; Strodel, P.; Koslowski, A.; Thiel, W.; Neese, F.; Frauenheim, T.; Elstner, M. *J. Phys. Chem. B* **2005**, *109*, 3606–3615.
36. Hoffmann, M.; Wanko, M.; Strodel, P.; König, P. H.; Frauenheim, T.; Schulten, K.; Thiel, W.; Tajkhorshid, E.; Elstner, M. *J. Am. Chem. Soc.* **2006**, *128*, 10808–10818.
37. Altun, A.; Kumar, D.; Neese, F.; Thiel, W. *J. Phys. Chem. A* **2008**, *112*, 12904–12910.
38. Altun, A.; Yokoyama, S.; Morokuma, K. *J. Phys. Chem. B* **2008**, *112*, 16883–16890.

# VII. Complete References from the Manuscript

R18. Frisch, M. J.; Trucks, G. W.; Schlegel, H. B.; Scuseria, G. E.; Robb, M. A.; Cheeseman, J. R.; Scalmani, G.; Barone, V.; Mennucci, B.; Petersson, G. A.; Nakatsuji, H.; Caricato, M.; Li, X.; Hratchian, H. P.; Izmaylov, A. F.; Bloino, J.; Zheng, G.; Sonnenberg, J. L.; Hada, M.; Ehara, M.; Toyota, K.; Fukuda, R.; Hasegawa, J.; Ishida, M.; Nakajima, T.; Honda, Y.; Kitao, O.; Nakai, H.; Vreven, T.; Montgomery, Jr., J. A.; Peralta, J. E.; Ogliaro, F.; Bearpark, M.; Heyd, J. J.; Brothers, E.; Kudin, K. N.; Staroverov, V. N.; Kobayashi, R.; Normand, J.; Raghavachari, K.; Rendell, A.; Burant, J. C.; Iyengar, S. S.; Tomasi, J.; Cossi, M.; Rega, N.; Millam, J. M.; Klene, M.; Knox, J. E.; Cross, J. B.; Bakken, V.; Adamo, C.; Jaramillo, J.; Gomperts, R.; Stratmann, R. E.; Yazyev, O.; Austin, A. J.; Cammi, R.; Pomelli, C.; Ochterski, J. W.; Martin, R. L.; Morokuma, K.; Zakrzewski, V. G.; Voth, G. A.; Salvador, P.; Dannenberg, J. J.; Dapprich, S.; Daniels, A. D.; Farkas, Ö.; Foresman, J. B.; Ortiz, J. V.; Cioslowski, J.; Fox, D. J. Gaussian, Inc., Wallingford CT, 2009.

R32. Cornell, W. D.; Cieplak, P.; Bayly, C. I.; Gould, I. R.; Merz, K. M.; Ferguson, D. M.; Spellmeyer, D. C.; Fox, T.; Caldwell, J. W.; Kollman. P. A. *J. Am. Chem. Soc.* **1995**, *117*, 5179.